HHS Public Access

Author manuscript

Biomaterials. Author manuscript; available in PMC 2016 June 01.

Published in final edited form as:

Biomaterials. 2015 June ; 53: 32–39. doi:10.1016/j.biomaterials.2015.02.038.

Tartaric Acid-based Amphiphilic Macromolecules with Ether Linkages Exhibit Enhanced Repression of Oxidized Low Density Lipoprotein Uptake

Dalia Abdelhamid[a,e,l], **Yingue Zhang**[a,l], **Daniel R. Lewis**[b], **Prabhas V. Moghe**[b,c], **William J. Welsh**[d], and **Kathryn E. Uhrich**[a,*]

[a]Department of Chemistry and Chemical Biology, Rutgers University, NJ, USA

[b]Department of Chemical and Biochemical Engineering, Rutgers University, NJ, USA

[c]Department of Biomedical Engineering, Rutgers University, NJ, USA

[d]Department of Pharmacology, Robert Wood Johnson Medical School, University of Medicine and Dentistry of New Jersey, Rutgers University, Piscataway, NJ, USA

[e]Department of Medicinal Chemistry, Faculty of Pharmacy, Minia University, Minia, Egypt

Abstract

Cardiovascular disease initiates with the atherogenic cascade of scavenger receptor- (SR-) mediated oxidized low-density lipoprotein (oxLDL) uptake. Resulting foam cell formation leads to lipid-rich lesions within arteries. We designed amphiphilic macromolecules (AMs) to inhibit these processes by competitively blocking oxLDL uptake via SRs, potentially arresting atherosclerotic development. In this study, we investigated the impact of replacing ester linkages with ether linkages in the AM hydrophobic domain. We hypothesized that ether linkages would impart flexibility for orientation to improve binding to SR binding pockets, enhancing anti-atherogenic activity. A series of tartaric acid-based AMs with varying hydrophobic chain lengths and conjugation chemistries were synthesized, characterized, and evaluated for bioactivity. 3-D conformations of AMs in aqueous conditions may have significant effects on anti-atherogenic potency and were simulated by molecular modeling. Notably, ether-linked AMs exhibited significantly higher levels of inhibition of oxLDL uptake than their corresponding ester analogues, indicating a dominant effect of linkage flexibility on pharmacological activity. The degradation stability was also enhanced for ether-linked AMs. These studies further suggested that alkyl chain length (i.e., relative hydrophobicity), conformation (i.e., orientation), and chemical stability play a critical role in modulating oxLDL uptake, and guide the design of innovative cardiovascular therapies.

*Corresponding Author: Kathryn E Uhrich, Professor, Department of Chemistry and Chemical Biology, Rutgers University, 610 Taylor Road, Piscataway, NJ 08854, Phone: 848-445-0361, FAX: 732-445-7036.

[l]These authors contributed equally to this work

Keywords

Amphiphilic macromolecule; atherosclerosis; self-assembled micelle; oxLDL uptake

1. Introduction

Cardiovascular diseases are the leading causes of mortality in developed countries.[1, 2] Atherosclerosis, characterized as the buildup of lipid rich plaques within the vascular intima, is the primary pathology underlying these conditions. Atherosclerosis starts with the accumulation of low-density lipoprotein (LDL) within blood vessel walls, where LDL undergoes oxidative modification.[3] The oxidized LDL (oxLDL) then triggers monocyte recruitment and differentiation into macrophages, which subsequently uptake oxLDL via scavenger receptors (SRs). This unregulated uptake of oxLDL leads to the formation of lipid-laden macrophages called foam cells and the secretion of inflammatory mediators.[4] The atherogenic accumulation of foam cells results in plaque buildup within artery walls, which can lead to myocardial infarction, stroke, or peripheral arterial disease.

Traditional cardiovascular therapies focus on lowering the hepatic synthesis of LDL to reduce the vascular lipid burden and mitigate atherosclerosis, however, they fail to target lesion sites and suffer from severe off-target effects.[5] An alternative approach to address atherosclerosis is through direct inhibition of oxLDL uptake via macrophage SRs, thus preventing the ensuing the inflammatory response. Previously, amphiphilic macromolecules (AMs) comprised of a branched hydrophobic domain and a hydrophilic tail (poly(ethylene glycol), PEG) were developed by our research group as biocompatible micelle-forming amphiphiles (representative structures shown in Figure 1A). These AMs have shown promising bioactivity as anti-atherogenic agents [6–9] by selectively blocking uncontrolled oxLDL uptake by macrophages.[7] By varying specific structural motifs of the AMs, the influence of several important features on anti-atherogenic activity was identified. These structural modifications included variations in the free carboxylic acid (location and numbers), nature of the backbone (stereochemistry), hydrophobic chains (number of branches and chain length), and PEG (molecular weight (Mw) and branching).[10, 11] Detailed studies have shown that seemingly minor changes in the stereochemistry, degree of branching, and/or hydrophobicity of the aliphatic chains have a considerable effect on bioactivity.[9, 12, 13] Molecular modeling studies further suggested that AMs competitively inhibit oxLDL uptake by SRs via electrostatic and hydrophobic interactions with SR binding domains.[14] The 3D conformation of AMs in aqueous conditions, specifically the presentation of the hydrophobic arms, appears to be critically important for this inhibition efficacy.[15]

While the influence of chain length and hydrophobic domain branching on bioactivity has been well established, the potential role of the linkage type between hydrophobic chains and backbones has not been systematically investigated. The ester linkages (Figure 1A) between the linear backbone and hydrophobic chains of previously investigated AMs are characterized by partial double bond character that limits freedom of movement. This conformational rigidity may govern the nature of AMs' corresponding three-dimensional

conformation, which ultimately affects the binding affinity of AMs to the SRs. We hypothesized that replacing ester linkages with ether linkages would increase the flexibility and overcome the rigidity challenges due to partial double bond resonance. We envisioned that the increased conformational flexibility afforded by the ether linkage would allow tighter alignment of the hydrophobic arms, rendering a better fit within the SR binding pocket and enhanced binding affinity.

Furthermore, susceptibility to esterase hydrolysis is an important consideration in drug design.[16] As the aforementioned ester linkages are vulnerable to esterase-catalyzed hydrolysis and degradation [17], we examined whether AMs with more stable ether linkages (Figure 1B) could overcome this potential limitation and thereby exhibit enhanced bioactivity. Bioavailability of ester conjugated AMs can be significantly reduced during blood circulation given the abundant presence of lipase (a subclass of esterases) in human serum[18], leading to compromised drug efficacy. As such, it is critical to design molecules that resist rapid degradation; this need also inspired our investigation of ether bonds, which are less susceptible to enzymatic hydrolysis.

In previous work, the most potent AM was based on a mucic acid backbone with ester-linked alkyl chains: M12P5 (Figure S1). As a proof of concept, in this study we designed novel ether-containing AM analogs based on a tartaric acid backbone with two hydrophobic chains (Figure 1B). Thus, for direct comparison and to clearly delineate the ester/ether effect, we also synthesized a tartaric acid-based ester-linked AM (Figure 1A). Herein, we present the synthetic strategy for preparing ether-linked AMs along with a detailed comparison of ether- and ester-linked AMs' physicochemical properties and biological activity. The enzymatic degradation stability of ether-linked AMs was also compared to ester-linked AMs, with the expectation that replacing ester linkages with more robust ether linkages would provide AMs with enhanced *in vivo* stability.

2. Materials and Methods

2.1. Materials

Reagents (tartaric acid, zinc chloride, lauroyl chloride, octyl chloride, decanoyl chloride, sodium hydride (NaH), bromooctane, bromodecane, bromododecane, dimethyl amino pyridine (DMAP), *p*-toluene sulphonic acid, N,N'-dicyclohexylcarbodiimide (DCC), monomethoxy-poly(ethylene glycol) (mPEG, Mn = 5000 Da), lipase from porcine pancreas, phosphate buffered saline (PBS, pH=7.4), and HPLC grade solvents were purchased from Sigma-Aldrich (Milwaukee, WI) and used directly unless otherwise mentioned. Lipase activity was determined using olive oil as a substrate following manufacturer protocols. (+) Dibenzyl L-tartrate was purchased from TCI (Duncan, SC). Dimethyl amino pyridine *p*-toluene sulphonate (DPTS) was prepared as previously published.[19] Polytetrafluoroethylene (PTFE) syringe filters were purchased from Fisher Scientific (Fair Lawn, NJ). Before use, 5k Da mPEG was azeotropically distilled with toluene (3×50 mL) and dried under high vacuum for 4 hours. 18 MΩ cm resistivity deionized (DI) water was obtained using PicoPure 2 UV Plus (Hydro Service and Supplies, Durham, NC). The following items were purchased from the indicated vendors: 1.077g/cm3 Ficoll-Paque Premium from GE healthcare (Pittsburgh, PA), RPMI 1640 from ATCC (Manassas, VA),

macrophage colony stimulating factor (M-CSF) from PeproTech (Rocky Hill, NJ), FBS from Life Technologies (Grand Island, NY), unlabeled oxLDL from Biomedical Technologies Inc. (Stoughton, MA), 3,3'-dioctadecyloxacarbocyanine (DiO) labeled oxLDL from Kalen Biomedical (Montgomery Village, MD), and human buffy coats from the Blood Center of New Jersey (East Orange, NJ).

2.2. Instrumentation

Chemical structures were confirmed by proton (^{1}H) and carbon (^{13}C) nuclear magnetic resonance (NMR) spectra, recorded on either a Varian 400 MHz or 500 MHz spectrometer. Samples were dissolved in deuterated chloroform ($CDCl_3$) containing tetramethylsilane (TMS) as an internal reference. Fourier transform infrared (FTIR) spectra were recorded on a Thermo Nicolet/Avatar 360 spectrophotometer using OMNIC software by solvent-casting samples in $CHCl_3$ onto a NaCl plate. Each spectrum was an average of 32 scans. Mass spectrometry was performed using ThermoQuest Finnigan LCQ-DUO system equipped with syringe pump, atmospheric pressure ionization (API) source, mass spectrometer (MS) detector, and X calibur data system. Samples were prepared in spectrophotometric grade methanol (MeOH) at a concentration of 10 μg/ml. AM Molecular weights (M_W) were determined by gel permeation chromatography (GPC) using a Waters LC system (Milford, MA) with a 2414 refractive index detector, a 1515 isocratic HPLC pump, and 717plus autosampler. HPLC grade tetrahydrofuran (THF) was used as eluent and for sample preparation. Samples (10 mg/mL) were dissolved in THF and filtered using 0.45 μm PTFE syringe filters before injection into the column at a flow rate of 1.0 mL/min. The average M_w of the sample was calibrated against narrow molecular weight PEG standards (Sigma-Aldrich, MI) on a Waters Stryagel® HR 3 THF column (7.8 × 300 mm). Melting temperature was determined using a TA instrument Q200 by heating samples (4–8 mg) under dry nitrogen gas from −30 °C to 200 °C. Data were collected at heating and cooling rates of 10 °C/min with a three-cycle minimum and analyzed using TA Instruments Universal Analysis 2000 software version 4.5 A. Hydrodynamic diameter and zeta potential measurements were determined using a Zetasizer nanoseries ZS90 (Malvern Instruments, UK). Samples (10 mg/mL) were prepared using HPLC grade water and filtered through 0.45 μm PTFE syringe filters before each measurement. Each sample was run three separate times at room temperature with 30 measurements per run. Critical micelle concentration (CMC) measurements were determined via fluorescence studies on a RF-5301PC spectrofluorometer (Shimadzu Scientific Instruments, Columbia, Maryland) at 25 °C.

2.3. Synthesis

2.3.1: General procedure for synthesis of alkylated benzyl tartrates (compounds 1 a – c)—Into an oven dried (cooled under Argon (g)) three necked round bottom flask (RBF), 10 mL anhydrous dimethylformamide (DMF) was added then cooled to −10 °C using an ice/salt bath. NaH (636 mg, 8.0 mmol) was slowly added following by dropwise addition of a dibenzyltartrate solution (1.36 g, 4.0 mmol in 10 mL anhydrous DMF) over 15 minutes. The reaction was stirred for 30 minutes, then the alkylating reagent (bromoalkane, 8.4 mmol) was added. The reaction was allowed to warm to room temperature and stirred for 16 hours. The reaction was quenched with saturated ammonium chloride (NH_4Cl) solution and extracted with ethyl acetate (3 × 15 mL). Combined organic

layers were dried over anhydrous sodium sulfate (Na_2SO_4). After filtration and solvent evaporation to dryness, the product was isolated by flash column chromatography using 95:5 hexane:ethyl acetate as the eluent.

Compound 1a: Colorless oil (244 mg, 11%). IR (cm^{-1}, thin film from $CHCl_3$): 2926, 2855, 1761, 1735. ^{1}H-NMR ($CDCl_3$): δ =7.34 (m, 10), 5.21 (d, 2), 5.15 (d, 2), 4.35 (s, 2), 3.70 (m, 2), 3.20 (m, 2), 1.47 (m, 4), 1.24 (m, 20), 0.86 (t, 6).^{13}C-NMR ($CDCl_3$):169.62, 135.65, 128.61, 80.24, 72.77, 67.02, 32.06, 29.57, 26.10, 22.87, 14.32. $[M + Na]^+_{theo}$= 577.7, GC-MS: $[M + Na]^+$= 577.8.

Compound 1b: Colorless oil (269 mg, 11%). IR (cm^{-1}, thin film from $CHCl_3$): 2924, 2854, 1762, 1734. ^{1}H-NMR ($CDCl_3$): δ = 7.33 (m, 10), 5.21 (d, 2), 5.15 (d, 2), 4.35 (s, 2), 3.70 (m, 2), 3.20 (m, 2), 1.47 (m, 4), 1.26 (m, 28), 0.86 (t, 6).^{13}C-NMR ($CDCl_3$):169.62, 135.66, 128.65, 80.24, 72.77, 67.02, 32.15, 29.68, 26.08, 22.93, 14.34.$[M + Na]^+_{theo}$= 633.8, GC-MS: $[M + Na]^+$= 633.3.

Compound 1c: Colorless oil (293 mg, 10%). IR (cm^{-1}, thin film from $CHCl_3$): 2924, 2853, 1762, 1735. ^{1}H-NMR ($CDCl_3$): δ = 7.33 (m, 10), 5.22 (d, 2), 5.14 (d, 2), 4.35 (s, 2), 3.71 (m, 2), 3.20 (m, 2),1.47 (m, 4), 1.24 (m, 20), 0.87 (t, 6).^{13}C-NMR ($CDCl_3$):169.62, 135.65, 128.76, 80.24, 72.77, 67.02, 32.15, 29.75, 26.10, 22.91, 14.34.$[M + Na]^+_{theo}$= 689.4, GC-MS: $[M + Na]^+$= 689.7.

2.3.2: General procedure for hydrogenolysis (compounds 2 a – c)—Alkylated dibenzyl tartrate (**1**, 0.5 mmol) was transferred into a RBF and dissolved in 10 mL anhydrous dichloromethane (DCM). 10 wt% Pd/C was added, and the reaction stirred under H_2 gas for 24 hours. Reaction progress was monitored by thin-layer chromatography (TLC) and after all starting material was consumed, the reaction mixture was filtered through a pad of celite and washed several times with DCM. Filtrate was concentrated *in vacuo* to obtain pure product (**2**).

Compound 2a: Colorless oil (180 mg, 96%). IR (cm^{-1}, thin film from $CHCl_3$): 2923, 2854, 1728. ^{1}H-NMR ($CDCl_3$): δ =4.37 (s, 2), 3.70 (m, 2), 3.51 (m, 2), 1.59 (m, 4), 1.26 (m, 20), 0.87 (t, 6).^{13}C-NMR ($CDCl_3$):171.16, 79.64, 73.86, 31.99, 29.57, 29.45, 29.37, 25.95, 22.84, 14.29. $[M + Na]^+_{theo}$= 397.5, GC-MS: $[M + Na]^+$ = 397.8.

Compound 2b: Colorless oil (204 mg, 95%). IR (cm^{-1}, thin film from $CHCl_3$): 3444, 2922, 2852, 1645. ^{1}H-NMR ($CDCl_3$): δ = 4.38 (s, 2), 3.70 (m, 2), 3.51 (m, 2), 1.60 (m, 4), 1.16 (bs, 28), 0.88 (t, 6).^{13}C-NMR ($CDCl_3$):170.98, 79.40, 73.68, 31.92, 29.71, 29.54, 29.37, 25.74, 22.68, 14.12.$[M + Na]^+_{theo}$= 453.6, GC-MS: $[M + Na]^+$ = 453.8.

Compound 2c: White solid (231 mg, 95 %). IR (cm^{-1}, thin film from $CHCl_3$): 2919, 2850, 1746. ^{1}H-NMR ($CDCl_3$): δ = 4.38 (s, 2), 3.69 (m, 2), 3.59 (m, 2), 1.47 (m, 4), 1.25 (m, 20), 0.88 (t, 6).^{13}C-NMR ($CDCl_3$): 169.60, 79.33, 73.88, 31.92,29.62, 29.48, 29.35, 25.73, 22.69, 14.12.$[M + Na]^+_{theo}$= 509.7, GC-MS: $[M + Na]^+$ = 509.9.

2.3.3: General procedure for coupling to PEG: (compounds 3 a – c)—Using an established literature procedure[19], PEG with 5 kDa Mw (0.28 g, 0.06 mmol) was dissolved in 2 mL anhydrous DCM. In a separate RBF, hydrogenolysis product (**2**, 0.18 mmol) and DPTS (0.02 g, 0.007 mmol) were dissolved in 2 mL anhydrous DCM and 0.5 mL anhydrous DMF under Argon, and this solution was added to the PEG solution. After 10 min stirring, DCC (1M in DCM) (0.19 mmol) was added dropwise to the reaction flask over 15 minutes via syringe. The reaction mixture was stirred at room temperature under Argon for 48 hours and the resulting white solid precipitate (DCC side product − dicyclohexylurea) was removed by vacuum filtration. The filtrate was washed with 0.1 N HCl (15 mL), then twice with brine (15 mL). The organic layer was dried over anhydrous Na_2SO_4 and evaporated to dryness. The crude product was purified by precipitation into diethyl ether (10 mL). The product was washed with diethyl ether (30 mL × 2) isolated by via centrifugation as a white solid.

Compound 3a: T(O-8)P5: White powder (0.20 g, 65%). ^{1}H-NMR ($CDCl_3$): δ = 4.32 (s, 2), 3.65 (m, ~500H), 1.68 (m, 8), 1.27(m, 20), 0.88 (t, 6); M_w = 5.2 kDa; PDI = 1.1.

Compound 3b: T(O-10)P5: White powder (0.22 g, 68%). ^{1}H-NMR ($CDCl_3$): δ = 4.32 (s, 2), 3.65 (m, ~500H), 1.70 (m, 8), 1.25 (m, 28), 0.88 (t, 6); M_w = 5.5 kDa; PDI = 1.1.

Compound 3c: T(O-12)P5: White powder (0.22 g, 67%). ^{1}H-NMR ($CDCl_3$): δ = 4.31 (s, 2), 3.65 (m, ~500H), 1.78 (m, 8), 1.25 (m, 36), 0.88 (t, 6); M_w = 5.2 kDa; PDI = 1.1.

2.3.4: General procedure for esterification: (compounds 4 a – c)—Compounds **4a** and **4b** were prepared in the same manner as the previously synthesized **4c** using a well established literature procedure[19]. Briefly, acid chloride (42 mL, 0.20 mol) was added to tartaric acid (4.0 g, 27 mmol) and zinc chloride (1.1 g, 8.0 mmol) in a 250 mL RBF. The reaction mixture was refluxed at 95 °C for 24 h. After cooling to room temperature, diethyl ether (20 mL) was added to the reaction mixture, and the solution was poured into ice water (150 mL) with stirring. Additional diethyl ether (80 mL) was added to the mixture and stirring continued for another 30 min. The ether portion was separated, washed three times with brine, dried over anhydrous Na_2SO_4, and evaporated to dryness. The crude product was purified by precipitation into cold hexane (200 mL) then filtered and dried under vacuum.

Compound 4a: Off-white powder (8.7 g, 56%). IR (cm^{-1}, thin film from $CHCl_3$): 3475, 2929, 1755, 1149. ^{1}H-NMR ($CDCl_3$): δ =5.75 (s, 2), 2.43 (m, 4), 1.63 (m, 4), 1.30 (m, 16), 0.88 (t, 6). ^{13}C-NMR ($CDCl_3$): 172.81, 70.23, 33.79, 31.82, 29.07, 29.03, 24.83, 22.78, 14.24. $[M + Na]^+_{theo}$= 425.2, GC-MS: $[M + Na]^+$ = 425.8.

Compound 4b: Off-white powder (8.7 g, 65%). IR (cm^{-1}, thin film from $CHCl_3$): 3461, 1647, 1219. ^{1}H-NMR ($CDCl_3$): δ = 5.75 (s, 2), 2.44 (m, 4), 1.64 (m, 4), 1.29 (m, 24), 0.88 (t, 6). ^{13}C-NMR ($CDCl_3$): 172.77, 70.23, 33.80, 32.07, 29.62, 29.48, 29.40, 29.16, 24.84, 22.88, 14.30. $[M + Na]^+_{theo}$= 481.2, GC-MS: $[M + Na]^+$ = 481.6.

2.3.5: General procedure for coupling to PEG: (compounds 5 a – c)—

Compounds **5a** and **5b** were prepared in the same manner as the previously synthesized **5c** [20], using **4a** or **4b** accordingly.

Compound 5a: T8P5: White powder (0.92g, 85%). ^{1}H-NMR (CDCl3): δ = 0.86 (t, 6), 1.26 (m, 32), 1.60 (b, 4), 2.39 (b, 4), 2.90 (s, 4), 3.41 (m, ~500H), 5.66 (s, 2); Mw = 5.5kDa; PDI = 1.1.

Compound 5b: T10P5: White powder (0.92g, 85%). ^{1}H-NMR (CDCl3): δ = 0.86 (t, 6), 1.26 (m, 32), 1.60 (b, 4), 2.39 (b, 4), 2.90 (s, 4), 3.41 (m, ~500H), 5.66 (s, 2); Mw = 5.5kDa; PDI = 1.1.

2.4. Critical micelle concentration (CMC) measurements

A solution of pyrene, a fluorescent probe, was made at a concentration of 5×10^{-6} M in acetone. Samples were prepared by adding 1 mL of pyrene solution to a series of vials and allowing the acetone to evaporate overnight. AMs were dissolved in HPLC grade water and diluted to a series of concentrations from 1×10^{-3} M to 1×10^{-10} M. AM solutions were then transferred to vials with the dry pyrene film and resulting AM-pyrene solutions (10 mL) were incubated at 37 °C for 24 hours to allow partitioning of the pyrene into micelles. The final concentration of pyrene in all samples was 5×10^{-7} M. Emission was performed from 300 to 360 nm, with 390 nm as the excitation wavelength. The maximum absorption of pyrene shifted from 332 to 334.5 nm upon partitioning into micelles.[21–23] The ratio of absorption of encapsulated pyrene (334.5 nm) to pyrene in water (332 nm) was plotted against the logarithm of polymer concentrations. The inflection point of the curve was taken as the CMC.

2.5. Isolation and culture of human monocyte derived macrophages (hMDMs)

Peripheral blood mononuclear cells (PBMCs) were isolated from human buffy coats and differentiated into macrophages, as previously described.[15] After differentiation, macrophages were trypsinized, scraped from flasks and transferred into well plates at 50,000 cells/cm^2. Macrophages were allowed to adhere for 24 hours before treatments were administered.

2.6. oxLDL uptake

To measure AM efficacy in inhibiting oxLDL uptake, hMDMs were incubated with 5 μg/mL oxLDL (1 μg/mL DiO labeled, 4 μg/mL unlabeled) and 10^{-6} M AMs in RPMI 1640 for 24 h. Following treatment, hMDMs were removed from plates by vigorous pipetting in cold PBS with 2 mM EDTA, centrifuged, and fixed in 1% paraformaldehyde. Uptake of fluorescently labeled oxLDL (DiO) was quantified using a FACS calibur flow cytometer (Beckton Dickenson, Franklin Lakes, NJ). A minimum of 10,000 macrophages per sample was collected, and quantified using the geometric mean fluorescence intensity (MFI) of oxLDL fluorescence associated with the hMDMs using FlowJo software (Treestar, Ashland, OR). Results represent the mean of four independent experiments. Data is presented as % oxLDL uptake, which was calculated using the following formula: % oxLDL uptake = 100*(MFI of AM containing condition)/(MFI of oxLDL control)

2.7. Foam cell formation

To measure foam cell formation, hMDMs were incubated with 50 μg/mL oxLDL and 10^{-5} M AMs in RPMI 1640 for 24 hours before fixation in 4% paraformaldehyde. Cells were washed with 60% isopropanol, stained with 3 mg/mL Oil Red O (ORO) in 60% isopropanol for 5 min and counterstained with Hoechst 33342. ORO-stained hMDMs were imaged on a Nikon Eclipse TE2000S using a 40× objective. Epifluorescent images of nuclei were merged with transmitted light images using ImageJ software (National Institutes of Health, Bethesda, MD).

2.8 Statistical analysis

All *in vitro* experiments were replicated a minimum of three times, using primary cells from distinct donors each time. Results are presented as mean ± standard error of the mean (S.E.M.) and data evaluated by one-way ANOVA and post-hoc Tukey's test for comparisons between multiple conditions. A p-value of 0.001 or less was considered statistically significant.

2.9. Molecular modeling

Molecular modeling calculations were performed on selected ester and ether AM model compounds to evaluate similarities and differences in conformational preferences. All operations were conducted using the *Spartan'08* molecular modeling software suite (version 4.0.0, build 131, Wavefunction, Inc., Irvine, CA). A total of four structural models were constructed and explored, representing model compounds for the respective ester and ether tartaric acid AMs as charge-neutral (-COOH) and anionic ($-COO^-$) species. The anionic forms depict the putative states that would exist under physiological pH conditions. In each case, the model compound structures were identical to the intact AMs under study, aside from the PEG tail which was truncated to five [-O-CH_2-CH2-] segments capped by a single [-O-CH_2-CH_3] group. Given our focus on the differential effects of the ester and ether linkages, these model compounds were considered sufficiently representative for this purpose. Preliminary calculations in which more PEG units were sequentially added to the tail revealed insignificant impact on our findings and, conversely, limited the number of physically meaningful conformers generated in conformational searches. Molecular mechanics calculations were carried out using the Merck Molecular Force Field (MMFF) [24] in an aqueous environment represented by the SM5.4 solvent model (MMFFaq).[25] A stochastic search of conformational space was implemented on each molecule using a Monte Carlo (MC) procedure that generated 10,000 independent conformers, from which the equilibrium (lowest energy) conformers were selected for subsequent visual inspection. This MC scheme employed a simulated annealing protocol that searches for the global low-energy conformer by biased sampling of low-energy conformers and high-energy conformers over the course of a pre-defined descending temperature gradient.

2.10. Lipase-catalyzed hydrolysis and degradation of AM micelles

Lipase-catalyzed degradation experiments were performed in the presence of lipase from porcine pancreas (30 U/mg). AM micelle solutions (3 mg/mL) in PBS (pH=7.4) were incubated with lipase at 3 U/mL at 37 °C with gentle agitation (60 RPM). 1.5 mL samples

were taken at predetermined time points up to 24 hours and extracted with DCM (3 × 2 mL). DCM was then removed *in vacuo*. The samples were dissolved in $CDCl_3$ and analyzed by ^{1}H-NMR for changes in chemical structure.

3. Results and Discussion

Synthesis of ether-linked AMs was completed in three steps: 1) alkylation of free hydroxyl groups of dibenzyl tartrate; 2) hydrogenolysis to remove the benzyl groups; and 3) coupling to PEG (Figure 2). Several experiments were performed to determine the optimal conditions (combination of suitable base and solvent) to accomplish the alkylation step. To our knowledge, this work is one of few papers discussing alkylation of vicinal hydroxyl groups with long chain alkyl halides (1-bromooctane/decane/dodecane).[26] Alkylation with long hydrophobic chains has not been well explored in literature and most procedures use reactive benzyl halides or small chain alkyl halides.[27] In our experiments, NaH in DMF gave the desired products in approximately 11% yield although complete deprotonation of -OH group by the base was confirmed by ^{1}H-NMR spectroscopy. This yield can be justified by the low reactivity of the halide and secondary alkoxide as well as the steric bulk of the long chain. Although it was reported that DMAP and triethylamine (TEA) work in DCM, only starting material was recovered using these reagents; similar low-yielding results were observed with sodium bis(trimethylsilyl)amide (NaHDMS) and lithium diisopropylamide (LDA). Hydrogenolysis of the benzyl esters was carried out with 10% w/w Pd/C in DCM and was quantitative. Approximately 65% yield of product (5**a–c**) was obtained after coupling PEG to the hydrophobes with DCC. Chemical structures of each compound were confirmed via ^{1}H-NMR, ^{13}C-NMR and FTIR spectroscopies, as well as MS or GPC.

Ester-linked AMs were prepared using procedures developed in our lab in relatively high yields (Figure 3).[19] Esterification of the vicinal hydroxyl groups in tartaric acid was performed using octanoyl/decanoyl/lauroyl chloride and zinc chloride as catalyst (56–65% yield). Afterwards, coupling to PEG using DCC in presence of DPTS as catalyst provided the final product (85% yield) after purification.

Measurements of melting temperatures (T_m), hydrodynamic radii, and CMC values demonstrated the impact of replacing ester backbone linkages with ether backbone linkages on thermal and solution properties, which may influence *in vivo* stability (Table 1). In both polymer classes, increasing the hydrophobic chain length slightly decreased the hydrodynamic radius. This observation is in accordance with the fact that increasing chain length enhances the van der Waal's interactions of hydrophobic chains which promote tighter alignment and, thereby, the formation of more compact micelles.[28] However, ether- and ester-linked AMs have comparable hydrodynamic size and zeta potential, possessing similar colloidal behavior. Interestingly, the CMC values of ether-linked AMs were one or two orders-of-magnitude lower than their corresponding ester-linked AM analogues, indicating an improved stability towards drastic dilution experienced upon systemic administration[29]. Given that the hydrophilic-lipophilic balance of the two AM classes was kept the same, aside from variance in backbone linkage types, it is plausible that the flexibility of linkages causes a difference in the packing of hydrocarbon arms during micellization, ultimately leading to the difference in CMC values. This was further explored

and investigated by molecular modeling, as will be discussed later. Notably, all synthesized AMs showed similar T*m* values, which suggests that thermal properties largely depend on the hydrophilic PEG domain (T*m* = 63°C) and is in consistent with previous observations. [11] In summary, ether-based AMs demonstrated enhanced solution stability over ester-based AMs while thermal properties were similar.

As described above, these new tartaric acid-based AMs with ether or ester bonds were developed to optimize biological activity. Their ability to inhibit oxLDL uptake and the resultant foam cell phenotype was therefore evaluated using human monocyte derived macrophages (hMDMs) (Figure 4). Macrophages incubated with ether-linked AMs showed significant reduction in oxLDL uptake levels as compared to their ester counterparts. All ester analog-treated conditions were not statistically different from the oxLDL alone treated cells, indicating they displayed little if any effect on inhibition of oxLDL uptake at the concentration tested. As anticipated, increased inhibitory efficacy directly correlated to hydrophobic chain length for ether-linked AMs. Previous studies also found that larger and more hydrophobic sugar derivatives resulted in higher levels of oxLDL uptake inhibition [12, 30]. This result is likely due to a higher affinity binding to the hydrophobic domain of SR binding pockets.

As foam cell formation is the major endpoint event in the atherogenic cascade, we also examined AMs' ability to prevent foam cell formation in hMDMs by blocking the unregulated internalization of oxidized lipids. Similar to oxLDL uptake studies, ether-linked AMs showed remarkable inhibition of lipid accumulation and were drastically more efficacious than ester-linked AMs (Figure 5). Cells treated with ether-linked AMs had minimal formation of intracellular lipid droplets, as evidenced by significant reduction of ORO-stained lipid droplets present, and maintained cell morphologies similar to basal controls. Ester-linked AM treated conditions displayed cell morphologies similar to oxLDL-only treated cells, including large lipid droplets and an enlarged phenotype. These results confirm that structural changes of the hydrophobic domain immensely impact AMs' ability to prevent development of foam and minor modifications in AM chemical structures can improve the biological activity.

In comparing the efficacy of ether-linked AMs to the most potent, previously developed AM M12P5 (Figure S1) similar levels of inhibitory activity were seen. Despite a smaller hydrophobic domain, the ether-linked AM **3c** was able to reduce oxLDL uptake by 90%, compared to an 85% reduction with M12P5.[15] Although hydrophobicity was previously shown to play a large role in determining AM efficacy, this study indicates that other factors also influence bioactivity.

To evaluate these factors, we adapted a previously developed molecular modeling framework to computationally screen biomaterials with anti-atherosclerotic properties.[15] Comparing AMs with the most hydrophobic (i.e., longest alkyl) chains, the molecular modeling studies reveal striking differences between the ester-linked **5c** and ether-linked AM **3c** in terms of their conformational features and overall molecular architectures. Initial calculations focused on the ester and ether as uncharged species (Figure 6A–B). For the ether-linked analog (**3c**, Figure 6A), the two alkyl side chains adopt a near parallel

alignment and are pointed away from the PEG tail. In sharp contrast, the corresponding ester-linked AM (**5c**, Figure 6B) alkyl side chains adopt an oblique orientation with an intersection angle of approximately 40°. The enhanced side chain alignment for the ether-linked compound (**3c**) may provide a more energetically favorable interaction with the hydrophobic binding pocket of the SR. This conformational disparity between the ether- and ester-linked AMs can be traced to differences in rotational flexibility between their corresponding linkers. The ether linkage is relatively small and quite flexible, which allows the two side chains to adopt a compact parallel alignment. In contrast, the ester linkage is rotationally less flexible due to steric crowding between the adjacent ester groups as well as partial double bond character and the bias toward an antiparallel orientation of their dipoles that directs the alkyl side chains in divergent directions. These observations are reflected in the CMC values: better alignment of the ether-linked AM correlates with a lower CMC value (Table 1: **3c** versus **5c**).

Inspection of the AM structures in such equilibrium conformations offers a glimpse into their configurations in aqueous solution. In both the ether- and ester-linked AMs, a strong hydrophilic interaction forms between the -COOH group and the PEG tail. Specifically, the -OH group of the carboxylic acid group engages in a hydrogen bond (O-H•••O distance 2.7Å) with backbone oxygen atoms in the PEG unit. This interaction of the hydrophilic -COOH and PEG moieties coincides with a dramatic bowing of the ether-linked AM such that the two lipophilic alkyl side chains and the hydrophilic COOH•••PEG dyad are oriented in opposite directions. Compared with the ester-linked AM (Figure 6B), the ether analog (Figure 6A) presents a more streamlined amphiphilic molecule that may facilitate its biological activity at membrane surfaces. This finding also suggests that the ether is more amenable than the ester to micelle formation, and would therefore possess a lower CMC as noted above.

The equilibrium conformations obtained from the MC search for the anionic forms ($COO^{2212;}$) of the ester and ether AMs closely resemble their arrangement in the corresponding uncharged forms (Figure 6C–D). Despite the absence of the -COOH•••PEG hydrogen bond, the solvated COO^{-} serves very much in the same capacity as the hydrogen bonding -OH of the -COOH head group to “seed” formation of the hydrophilic cluster with the PEG unit. Results from the present calculations demonstrate that seemingly minor changes in the structures of these AMs can translate to significant alterations in their physicochemical properties and biological activity.

Finally, as enzymatic degradation of AMs *in vivo* could significantly alter AM bioavailability and efficiency, the degradation stability of our AMs was carefully examined in the presence porcine pancreatic lipase by ^{1}H-NMR spectroscopy. To understand the influence of linkage types as well as hydrophobicity on the degradation rate of AMs, compounds **3c, 5c** and M12P5 were assessed at 37 °C and pH=7.4 to mimic physiological conditions (Figure 7). ^{1}H-NMR spectroscopy was used to monitor changes in AM chemical structure via the appearance of degradation products. While all three AMs have a hydrolysable ester bond between the hydrophilic PEG and the hydrophobic segment, compounds **5c** and M12P5 also have ester bonds between their alkyl arms and linear backbones in the hydrophobic region. Specifically, the CH_2 of the alkyl chain arms *alpha* to

ester carbonyl moieties (2.30 and 2.42 ppm for M12P5, and 2.41 ppm for **5c**) and the terminal CH_3 of ether-linked alkyl arms (0.88 ppm for **3c**) were monitored. For **3c**, the terminal CH_3 was analyzed instead of the CH_2 of the alkyl arms *alpha* to the ether linkages due to overlaps between the aforementioned CH_2 signal (~ 3.6 ppm) and broad PEG peaks (~ 3.4 – 4.2 ppm). The degradation of M12P5's hydrophobic domain was implied by the appearance of new CH_2 peaks at 2.35 ppm, correlating with hydrolysis of the ester bonds between alkyl arms and the linear backbones, releasing dodecanoic acid (Figure 7). The complete degradation of M12P5 took less than 3 h while complete degradation of **5c** was longer than 3 h. These observations suggest that M12P5 with higher level of hydrophobicity interacted more favorably with lipase, leading to an accelerated degradation. A similar observation has been reported for the enzymatic degradation of PEG_{45}-b-PCL_{60} micelles, indicating that more hydrophobic polymers undergo a more rapid degradation.[31] In contrast to both ester-linked AMs, negligible changes were observed for **3c**'s terminal CH_3 (0.88 ppm). The absence of a dodecanol degradation product, CH_3 peak at 0.77 ppm, further confirmed the robust stability of AMs with ether linkages in the hydrophobic region. Although **3c** exhibited comparable efficiency in reducing oxLDL uptake as M12P5, compound **3c** holds more promise for *in vivo* treatment with its resistance to rapid enzymatic degradation. The bioactivity of AMs with lipase degradation treatment is under further investigated, along with additional studies evaluating their viability for commercialization; these results will be discussed in a future publication.

4. Conclusions

Novel ether- and ester-linked AMs were designed and synthesized to investigate the impact of linkage type between alkyl arms and linear backbones on biological activity and physicochemical properties. Similar physicochemical properties were observed for both classes, however, ether-linked AMs displayed significantly higher ability to inhibit oxLDL uptake and foam cell formation – two key steps in atherosclerosis. Furthermore, molecular modeling studies suggest that the higher activity may be attributed to the increased flexibility of the ether linkage and better alignment of alkyl arms, which facilitates hydrogen-bonding of the sugar carboxylate with the hydrophilic PEG tail. Finally, the leading ether-linked AM demonstrated enhanced stability towards enzymatic degradation over that of our gold standard, in addition to its comparable bioactivity. Data generated in this study provide valuable insights regarding the design of potent AMs for the treatment of cardiovascular disease.

Supplementary Material

Refer to Web version on PubMed Central for supplementary material.

Acknowledgments

This study was supported by NIH grants (R21093753 to PVM and NIH grant R01 HL107913 to PVM and KEU). The authors would like to thank Qi Li for technical help.

References

1. Li AC, Glass CK. The macrophage foam cell as a target for therapeutic intervention. Nat Med. 2002; 8:1235–1242. [PubMed: 12411950]
2. Lloyd-Jones D, Adams RJ, Brown TM, Carnethon M, Dai S, De Simone G, et al. Heart disease and stroke statistics-2010 update: a report from the American Heart Association. Circulation. 2010; 121:e46–e215. [PubMed: 20019324]
3. Itabe H. Oxidative modification of LDL: its pathological role in atherosclerosis. Clinical reviews in allergy & immunology. 2009; 37:4–11. [PubMed: 18987785]
4. Yoshimoto T, Takahashi Y, Kinoshita T, Sakashita T, Inoue H, Tanabe T. Growth stimulation and epidermal growth factor receptor induction in cyclooxygenase-overexpressing human colon carcinoma cells. Advances in experimental medicine and biology. 2002; 507:403–407. [PubMed: 12664617]
5. Maron DJ, Fazio S, Linton MF. Current perspectives on statins. Circulation. 2000; 101:207–213. [PubMed: 10637210]
6. Chnari E, Nikitczuk JS, Uhrich KE, Moghe PV. Nanoscale anionic macromolecules can inhibit cellular uptake of differentially oxidized LDL. Biomacromolecules. 2006; 7:597–603. [PubMed: 16471936]
7. Chnari E, Lari HB, Tian L, Uhrich KE, Moghe PV. Nanoscale anionic macromolecules for selective retention of low-density lipoproteins. Biomaterials. 2005; 26:3749–3758. [PubMed: 15621265]
8. Iverson NM, Plourde NM, Sparks SM, Wang J, Patel EN, Shah PS, et al. Dual use of amphiphilic macromolecules as cholesterol efflux triggers and inhibitors of macrophage athero-inflammation. Biomaterials. 2011; 32:8319–8327. [PubMed: 21816466]
9. Iverson NM, Sparks SM, Demirdirek B, Uhrich KE, Moghe PV. Controllable inhibition of cellular uptake of oxidized low-density lipoprotein: structure-function relationships for nanoscale amphiphilic polymers. Acta biomaterialia. 2010; 6:3081–3091. [PubMed: 20170758]
10. Iverson NM, Sparks SM, Demirdirek B, Uhrich KE, Moghe PV. Controllable inhibition of cellular uptake of oxidized low-density lipoprotein: Structure-function relationships for nanoscale amphiphilic polymers. Acta Biomater. 2010; 6:3081–3091. [PubMed: 20170758]
11. Abdelhamid D, Arslan H, Zhang Y, Uhrich KE. Role of Branching of Hydrophilic Domain on Physicochemical Properties of Amphiphilic Macromolecules. Polymer chemistry. 2014; 5:1457–1462. [PubMed: 24533034]
12. Poree DE, Zablocki K, Faig A, Moghe PV, Uhrich KE. Nanoscale amphiphilic macromolecules with variable lipophilicity and stereochemistry modulate inhibition of oxidized low-density lipoprotein uptake. Biomacromolecules. 2013; 14:2463–2469. [PubMed: 23795777]
13. Hehir S, Plourde NM, Gu L, Poree DE, Welsh WJ, Moghe PV, et al. Carbohydrate composition of amphiphilic macromolecules influences physicochemical properties and binding to atherogenic scavenger receptor A. Acta biomaterialia. 2012; 8:3956–3962. [PubMed: 22835678]
14. Plourde NM, Kortagere S, Welsh W, Moghe PV. Structure-activity relations of nanolipoblockers with the atherogenic domain of human macrophage scavenger receptor A. Biomacromolecules. 2009; 10:1381–1391. [PubMed: 19405544]
15. Lewis DR, Kholodovych V, Tomasini MD, Abdelhamid D, Petersen LK, Welsh WJ, et al. In silico design of anti-atherogenic biomaterials. Biomaterials. 2013; 34:7950–7959. [PubMed: 23891521]
16. Casey Laizure S, Herring V, Hu Z, Witbrodt K, Parker RB. The Role of Human Carboxylesterases in Drug Metabolism: Have We Overlooked Their Importance? Pharmacotherapy: The Journal of Human Pharmacology and Drug Therapy. 2013; 33:210–222.
17. Demirdirek, B. “Synthesis and Evaluation of Amphiphilic Scorpion-like and Star Macromolecules for Biomedical Applications”. Rutgers: The State University of New Jersey; 2009.
18. Tietz N, Shuey D. Lipase in serum--the elusive enzyme: an overview. Clinical chemistry. 1993; 39:746–756. [PubMed: 8485865]
19. Tian L, Yam L, Zhou N, Tat H, Uhrich KE. Amphiphilic scorpion-like macromolecules: Design, synthesis, and characterization. Macromolecules. 2004; 37:538–543.
20. Tao L, Uhrich KE. Novel amphiphilic macromolecules and their in vitro characterization as stabilized micellar drug delivery systems. J Colloid Interf Sci. 2006; 298:102–110.

21. Astafieva I, Zhong XF, Eisenberg A. Critical Micellization Phenomena in Block Polyelectrolyte Solutions. Macromolecules. 1993; 26:7339–7352.
22. Meng FB, Zhang BY, Lian J, Wu YP, Li XZ, Yao DS. Mesomorphic Behavior and Optical Properties of Liquid-Crystalline Polysiloxanes Bearing Different Chiral Groups. J Appl Polym Sci. 2009; 114:2195–2203.
23. Kalyanasundaram K, Thomas JK. Environmental effects on vibronic band intensities in pyrene monomer fluorescence and their application in studies of micellar systems. Journal of the American Chemical Society. 1977; 99:2039–2044.
24. Halgren TA. Merck molecular force field. I. Basis, form, scope, parameterization, and performance of MMFF94. Journal of Computational Chemistry. 1996; 17:490–519.
25. Chambers CC, Hawkins GD, Cramer CJ, Truhlar DG. Model for Aqueous Solvation Based on Class IV Atomic Charges and First Solvation Shell Effects. The Journal of Physical Chemistry. 1996; 100:16385–16398.
26. Walton J, Tiddy GJT, Webb SJ. Synthesis and lyotropic phase behavior of novel nonionic surfactants for the crystallization of integral membrane proteins. Tetrahedron Letters. 2006; 47:737–741.
27. Kumar S, Ramachandran U. An improved procedure for the etherfication of α-hydroxy acid derivatives. Organic Preparations and Procedures International. 2004; 36:380–383.
28. Yang JS, Zhou QQ, He W. Amphipathicity and self-assembly behavior of amphiphilic alginate esters. Carbohydrate polymers. 2013; 92:223–227. [PubMed: 23218287]
29. Allen C, Maysinger D, Eisenberg A. Nano-engineering block copolymer aggregates for drug delivery. Colloids and Surfaces B: Biointerfaces. 1999; 16:3–27.
30. Faig A, Petersen LK, Moghe PV, Uhrich KE. Impact of Hydrophobic Chain Composition on Amphiphilic Macromolecule Antiatherogenic Bioactivity. Biomacromolecules. 2014; 15:3328–3337. [PubMed: 25070717]
31. Zhu X, Fryd M, Wayland BB. Kinetic-mechanistic studies of lipase-polymer micelle binding and catalytic degradation: Enzyme interfacial activation. Polymer Degradation and Stability. 2013; 98:1173–1181.

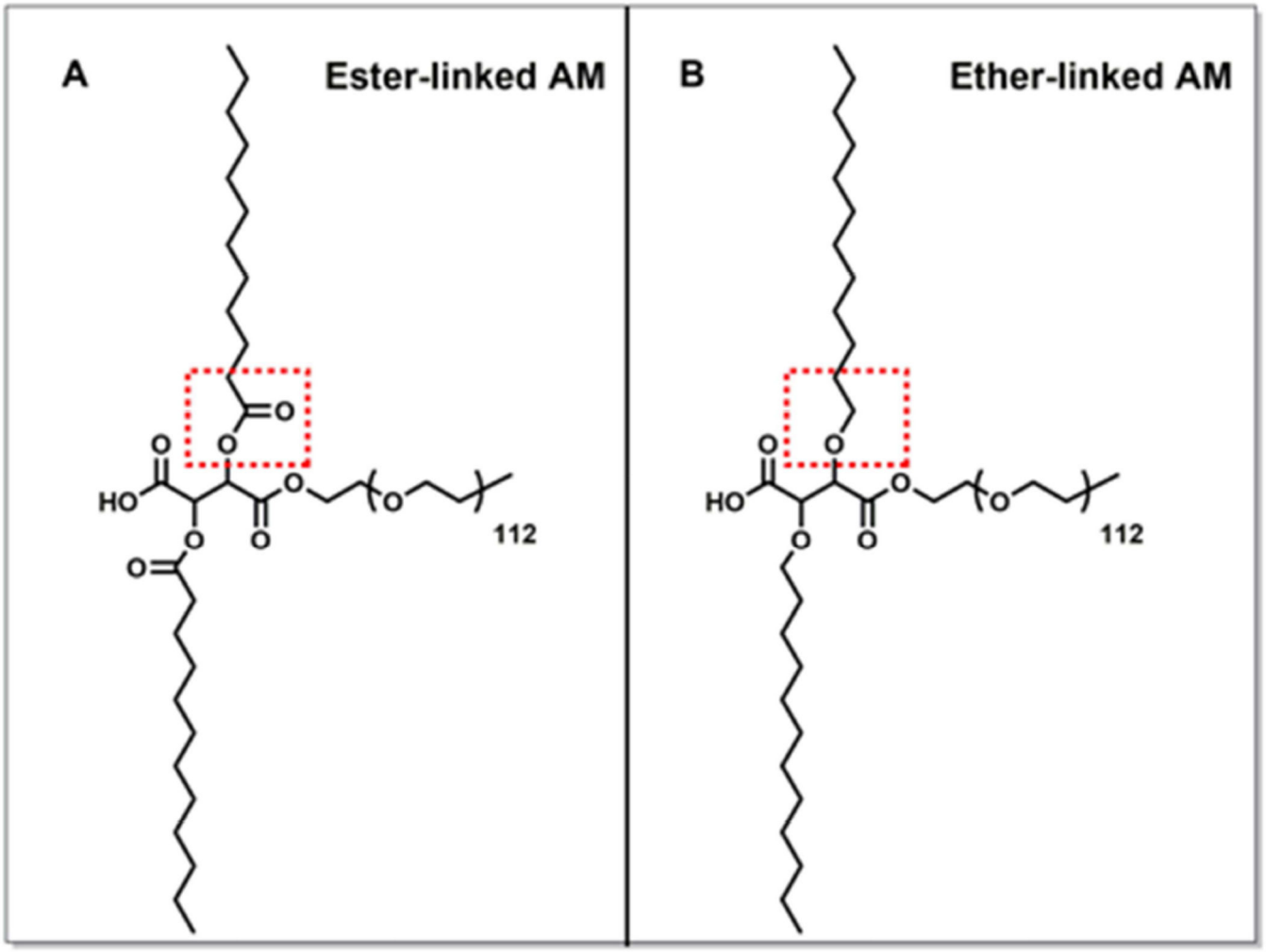

Figure 1.

Representative chemical structure of AMs based on tartaric acid backbone with ester linkages (A) and corresponding analogs with ether linkages (B).

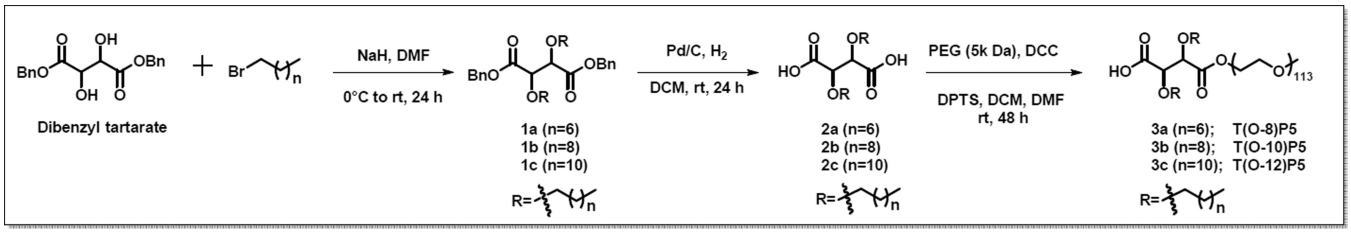

Figure 2.
Scheme for synthesis of the ether analogs

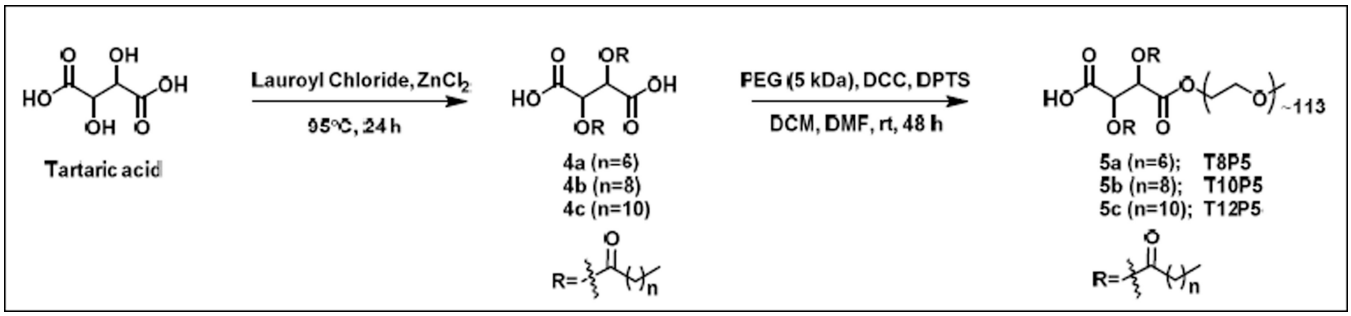

Figure 3.
Scheme for synthesis of the ester analogs

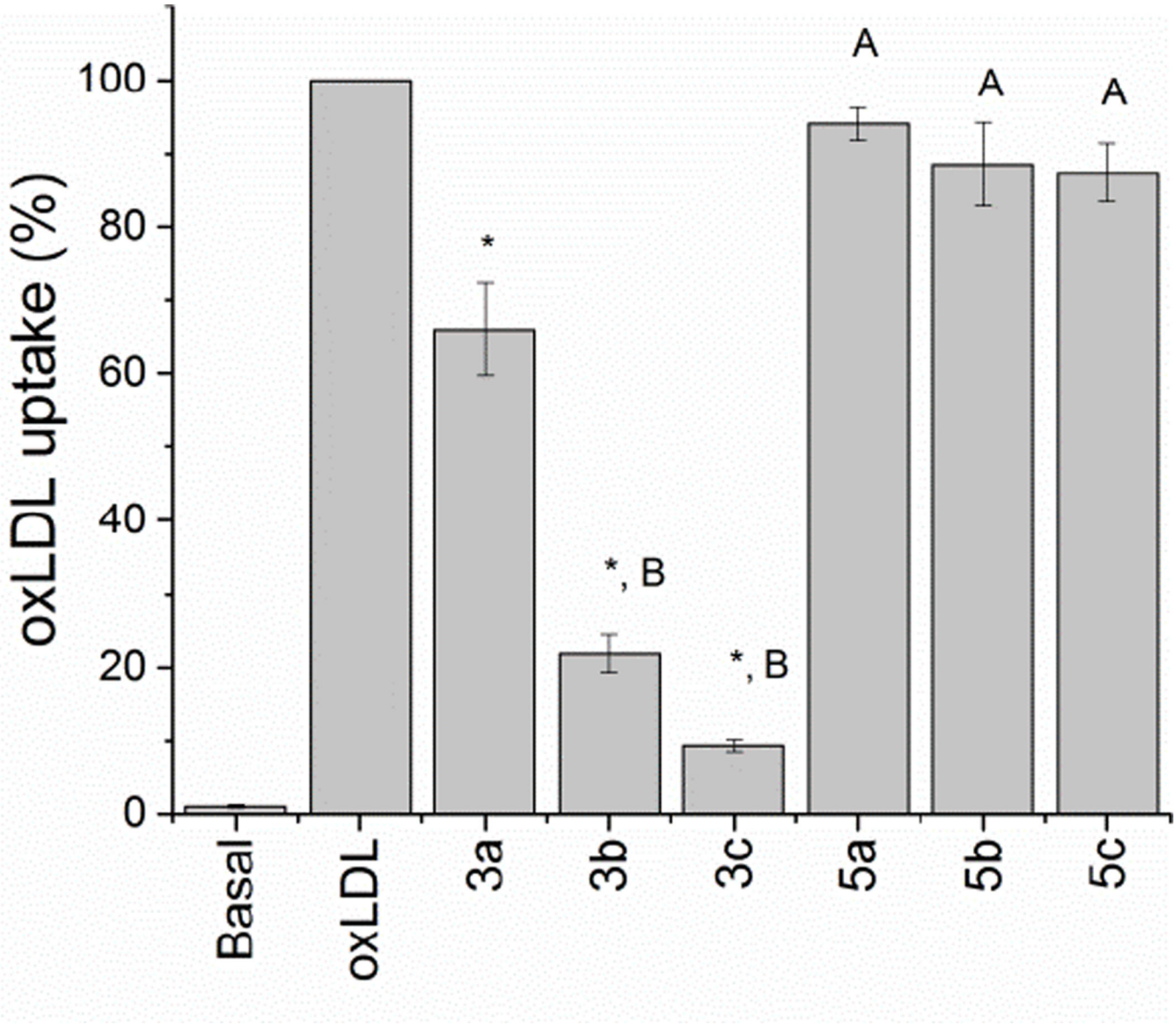

Figure 4.

oxLDL uptake inhibition by AMs in hMDMs. All ether-linked AMs had significant reductions in oxLDL uptake, with increased efficacy being directly correlated to longer aliphatic chains. hMDMs were incubated with 5 μg/mL oxLDL and 10^{-6} M AMs in RPMI 1640 for 24 h then analyzed via flow cytometry. * corresponds to $p<0.001$ relative to oxLDL control, same letter denotes conditions that were not statistically different.

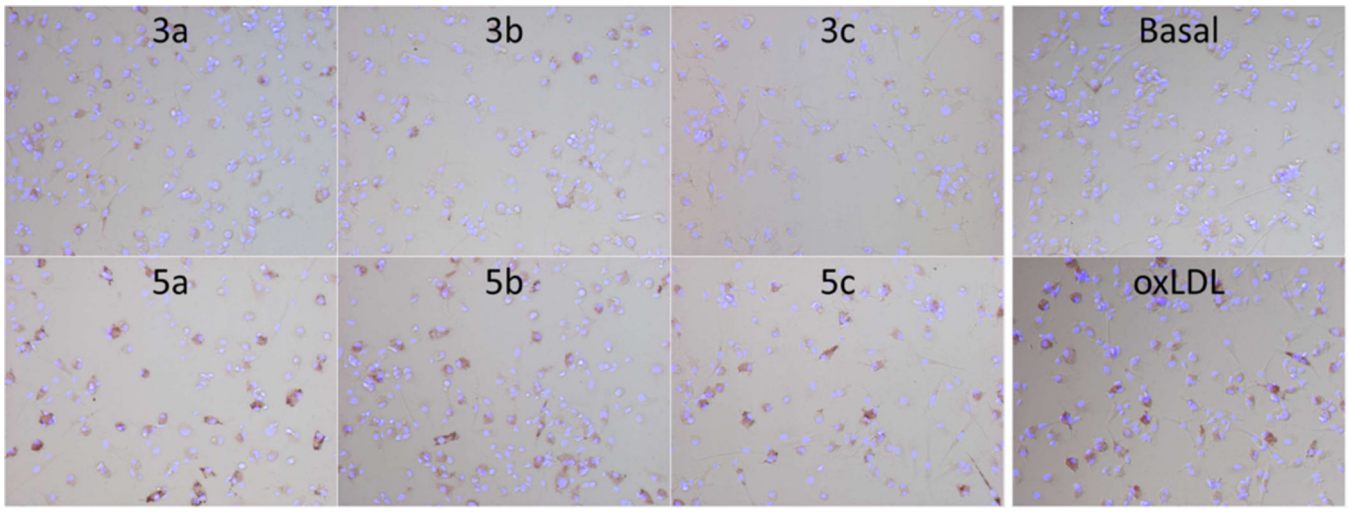

Figure 5.

Foam cell formation in hMDMs. Similar to oxLDL uptake studies, ether-linked AMs (**3**) displayed significantly higher efficacy than ester-linked AMs (**5**) at preventing the foam cell phenotype from developing, minimizing intracellular lipid accumulation. hMDMs were incubated with 50 μg/mL oxLDL and 10^{-5} M AMs in RPMI 1640 for 24 h before staining with Oil Red O and Hoechst 33342.

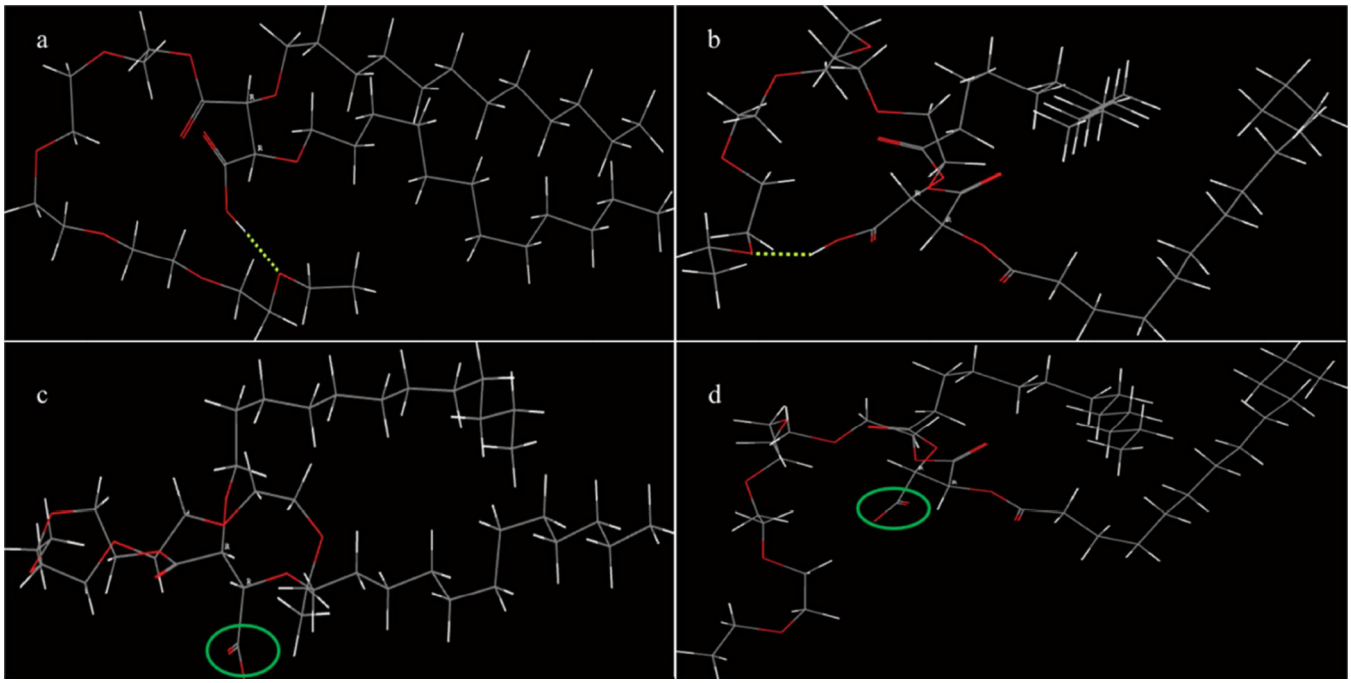

Figure 6.

Computer snapshots of equilibrium (low-energy) conformer of the subject AMmodel compounds (Left: ether-linked AM 3c. Right: ester-linked AM 5c) as neutral (uncharged) species (a–b) and anionic (negatively charged) species (c–d) from MC simulations. Atoms are color-coded: C (gray), H (white), O (red). The yellow dashed line depicts an OH---O hydrogen bond. For the ester analog, the uppermost C12-aliphatic side chain is projecting outward toward the viewer. The COO- anion, circled in green, is directed toward the aqueous media in the vicinity of the PEG tail.

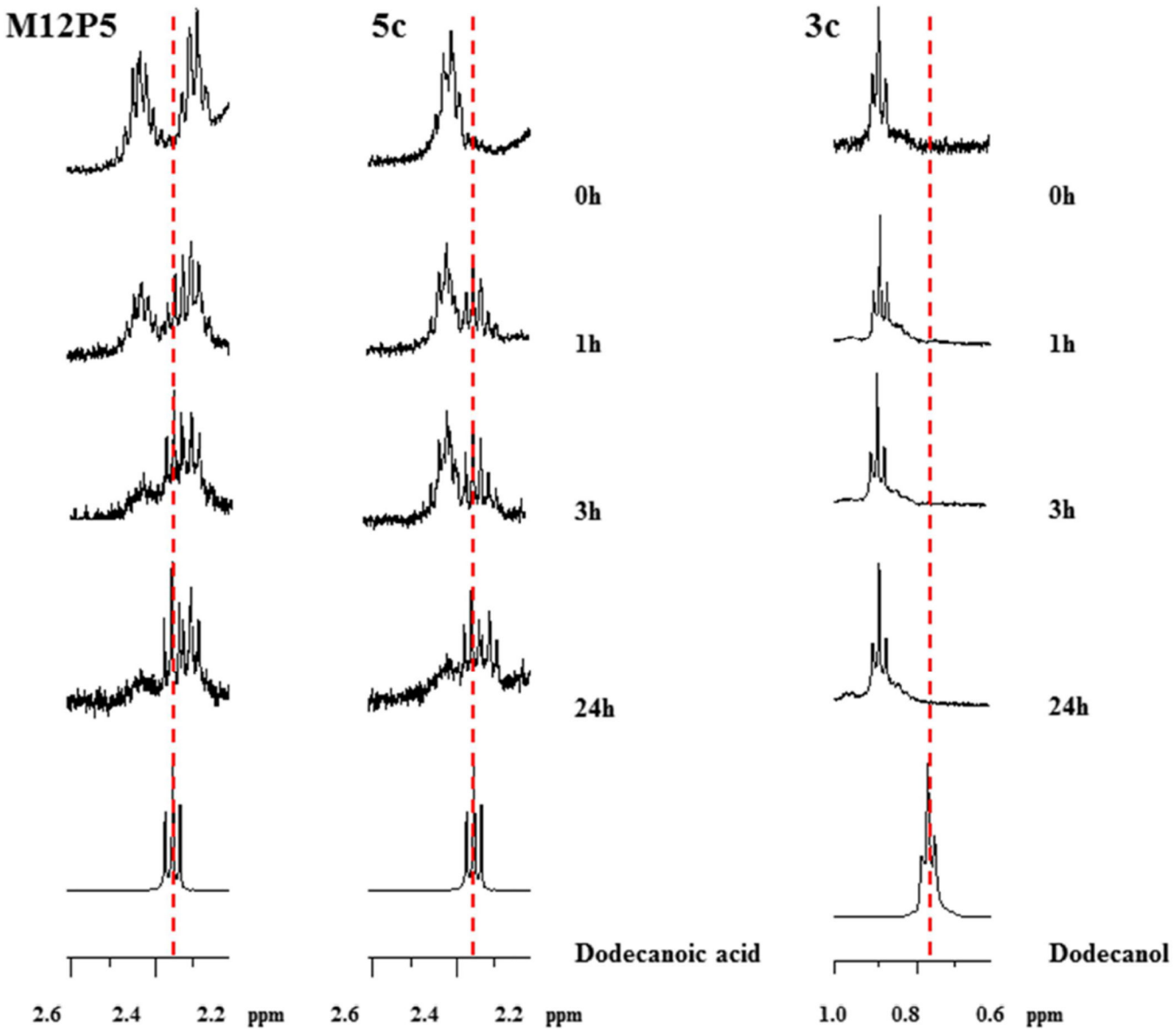

Figure 7.

Porcine pancreatic lipase catalyzed degradation of ester-linked AMs (M12P5 and **5c**) and ether-linked AMs (**3c**) at an activity of 3 U/mL.

Table 1

Physicochemical properties of synthesized ether- and ester- AMs

	Ether-linked AMs			Ester-linked AMs		
	3a	**3b**	**3c**	**5a**	**5b**	**5c**
Hydrodynamic size (nm)	22	20	18	23	18	15
Zeta potential (mV)	0.4	−1.8	−2.1	−2.8	−1.8	−1.9
Tm (°C)	54–57	54–57	55–57	54–56	52–57	55–57
CMC (mol/L)	5.0×10^{-7}	5.1×10^{-6}	8.9×10^{-6}	6.6×10^{-5}	6.4×10^{-5}	6.5×10^{-5}